nature chemistry

SUPPLEMENTARY INFORMATION

DOI: 10.1038/NCHEM.1622

Single-nanoparticle phase transitions visualized by four-dimensional electron microscopy

Renske M. van der Veen[‡], *Oh-Hoon Kwon*[‡], *Antoine M. Tissot*[¶], *Andreas Hauser*[¶], *and Ahmed H. Zewail*[‡]*

[‡]*Physical Biology Center for Ultrafast Science and Technology*

Arthur Amos Noyes Laboratory of Chemical Physics

California Institute of Technology, Pasadena, CA 91125, United States

[¶]*Département de Chimie Physique*

Université de Genève, CH-1211 Genève, Switzerland

*To whom correspondence should be addressed:

Email: zewail@caltech.edu

S1 Details of the phase-transition fitting procedures

The phase transition curves in Fig. 3c and 3f were fitted to a sigmoid function:

$$f(x) = base + \frac{max}{1 + e^{\frac{xhalf - x}{\Delta T}}}$$

where *base* is the momentum transfer value of the low-spin state, *max* is the amplitude of the phase transition change, *xhalf* is the center temperature of the curve, and ΔT is its slope. The following table provides the fitted parameters and fitting errors (standard deviations):

	Single nanoparticle		*Ensemble*	
	Heating	Cooling	Heating	Cooling
***base* /nm^{-1}**	1.9638 ± 0.001	1.9628 ± 0.001	1.9603 ± 0.001	1.9623± 0.001
***max* /nm^{-1}**	-0.043 ± 0.002	-0.041 ± 0.002	-0.045 ± 0.001	-0.047± 0.001
***xhalf* / K**	253 ± 5	241 ± 4	247 ± 2	231 ± 2
ΔT / K	31 ± 4	28 ± 4	15 ± 2	18 ± 2

The vertical error bar in the bottom left corner of Fig. 3f was estimated from the data scatter above and below the phase transition. We estimate it to be approximately ±0.002 nm^{-1}, which is used as a weighting factor in the curve fitting. Note that one pixel on the CCD corresponds to 0.007-0.008 nm^{-1} (depending on the camera length). The diffraction peak fitting errors are much smaller (<<pixel) than the systematic errors in the measurements.

To within our experimental error, the hysteresis widths are similar (12±6 K for the single particle; 16±3 K for the ensemble). However, the larger ΔT values for the single-nanoparticle shows that its phase transition is shallower.

S2 Sample characterization measurements

S2.1 X-ray powder diffraction

A powder X-Ray diffraction pattern was recorded at room temperature on the Fe(pyrazine)Pt(CN)$_4$.2H$_2$O nanoparticles before any thermal treatment (see Fig. S1). The obtained pattern is fully coherent with the previously reported one, confirming the crystallinity and the purity of the nanoparticles. [1]

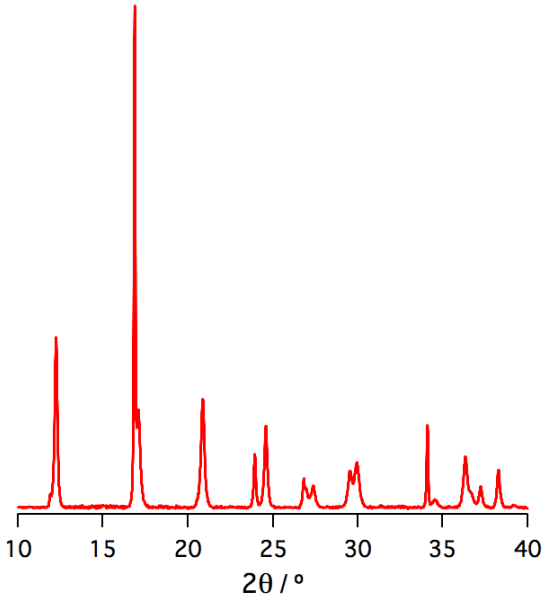

Figure S1. Powder X-Ray diffraction pattern of Fe(pyrazine)Pt(CN)$_4$.2H$_2$O nanoparticles.

Thermogravimetric measurement performed on the nanoparticles show a 7.8% weight loss between RT and 400 K, consistent with the loss of the two water molecules per formula unit. Therefore, a similar thermal treatment (2 hours at 400 K) was applied to the nanoparticle powder before other measurements in order to study the fully dehydrated Fe(pyrazine)Pt(CN)$_4$ compound.

S2.2 Optical spectroscopy measurements

Optical measurements were performed in order to study the thermal and photo-induced spin-transition behaviour of an ensemble of nanoparticles. For these

measurements, the nanoparticle powder was dispersed in ethanol and sonicated for 20 s. Droplets of the solution were delivered on a sapphire disk to obtain a yellow film. Before any measurement, the disk was heated up to 400 K during 2 hours to remove the crystal water. The disk was then placed on a home-built sample holder and cooled down with a closed-cycle He cryostat.

The temperature dependence of the optical absorption is shown in Fig. S2. At 293 K, an MLCT absorption band located at 470 nm, characteristic of the HS state, is detected. Upon cooling the sample to 60 K, a more intense MLCT absorption band, centered at 550 nm, appears. This change in the absorption spectra is a consequence of the HS-LS transition, and therefore, a spin transition curve can be extracted from a series of temperature-dependent optical spectra by following the evolution of the absorption at 570 nm. The thermal spin transition is located at around 250 K and a 8 K wide hysteresis loop is observed (T_{up} = 254 K, T_{down} = 246 K). The phase transition behavior as measured with electron diffraction in the TEM (Fig. 3c and 3d in the main article) is in good agreement with these measurements.

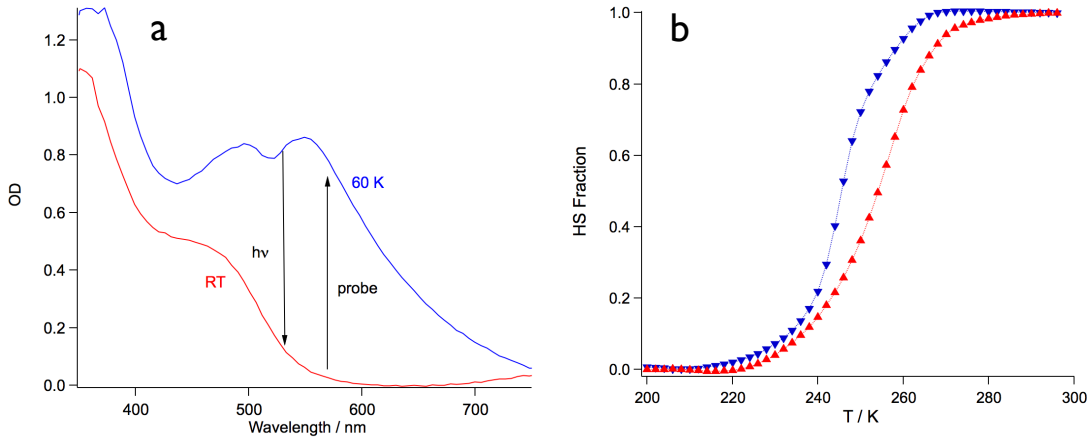

Figure S2. (a) UV/vis spectra of the LS and HS states measured at 60 K and RT, respectively. Vertical arrows indicate the excitation and probing wavelengths. (b) Thermal spin transition curve obtained by monitoring the absorption at 570 nm as a function of temperature during heating (red) and cooling (blue) cycle.

Time-resolved transient absorption measurements were performed in order to probe the HS→LS relaxation kinetics at different temperatures. Photo-excitation was performed using the second harmonic of a pulsed Nd:YAG Laser (532 nm, pulse duration: 7 ns, pulse energy: 1 – 8 mJ). The HS-LS relaxation was probed with the light of a Xenon lamp at 570 nm using a single monochromator (Spex 270M), a photomultiplier (Hamamatsu R928) and a digital oscilloscope (Tektronix TDS 540B). In a first step, the pulse energy was optimized in order to get the highest photoconversion rate possible without getting any detectable heating effect (i.e. around 3 mJ/pulse or 24 mJ/cm^2). Indeed, when the laser power was set above 3 mJ/pulse, a fast relaxation process, occurring within a few µs with a strongly laser power dependent intensity was detected and attributed to heating effects.

Relaxation curves were monitored at different temperatures and fitted with a single exponential decay model in order to obtain the relaxation rate constant $k_{HL}(T)$. An Arrhenius plot ($\log(k_{HL}(T))$ vs. 1/T, Figure S3b) was then used to extract the kinetic parameters associated with the HS→LS relaxation in the thermally activated region (i.e. above 60 K).

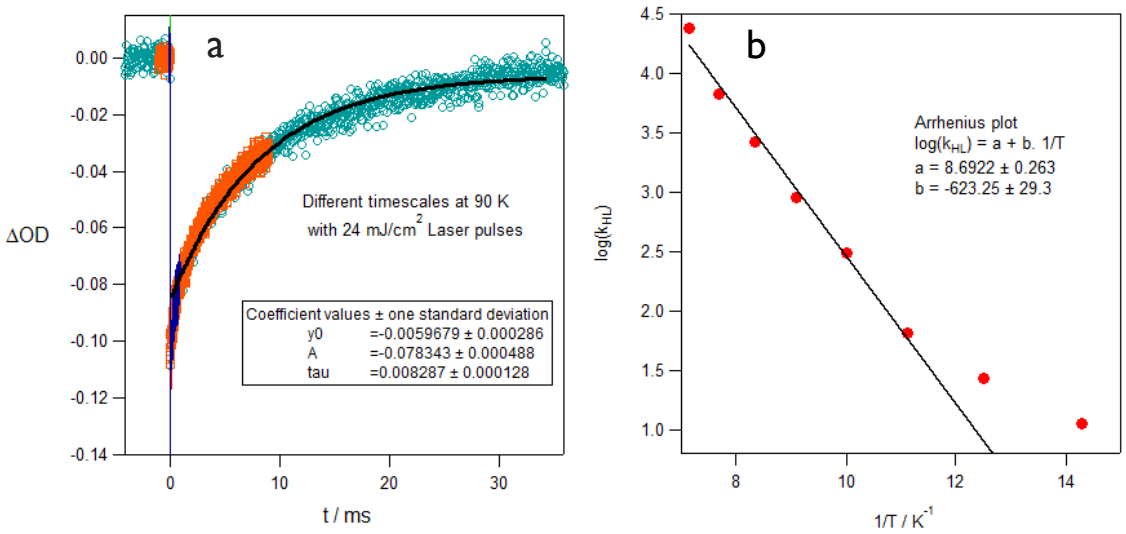

Figure S3. (a) HS→LS relaxation at 90 K. The decay was fitted with a single exponential (τ = 8.2±0.1 ms). (b) Arrhenius plot obtained from measuring the HS→LS relaxation rate at different temperatures.

S3 Time profile fitting

The diffraction time profiles were fitted with the following function:

$$f(t) = IRF \otimes \left[A \cdot Step \cdot e^{-\frac{(t-t_0)}{\tau_{decay}}} - A \cdot Step \cdot e^{-\frac{(t-t_0)}{\tau_{rise}}} + B \cdot Step \right]$$

where A is the amplitude of the change, t_0 is the time zero (for which the laser and electron pulses overlap in time), τ_{decay} is the partial recovery time of the diffraction signal, τ_{rise} is the initial rise/drop time and B is the amplitude of the long-lived signal (assuming infinite decay time within the measurement time window). *Step* is a Heaviside step function and *IRF* represents the instrumental response function, which we assume to be Gaussian with a FWHM of 15 ns (fixed in the fits). The decay and rise times are provided in the text (with their respective standard deviations).

S4 Additional nanoparticle dynamics

Fig. S4 shows the comparison between two nanoparticles under identical excitation conditions: NP A is the same as the nanoparticle of Figs. 4 and 5 in the main manuscript. NP B is a particle that lies on the same graphite substrate; both particles lie about 1 μm away from the Cu grid. NP B exhibits slower dynamics because it is larger and thicker. In addition, the particle seems to lie on top of another particle, which could reduce the thermal contact (making the heating and cooling dynamics slower as well). The slower cooling dynamics gives the particle more time to relax back to the LS state, which results in a smaller trapped HS component than for NP A (similar as was observed for the ensemble of nanoparticles).

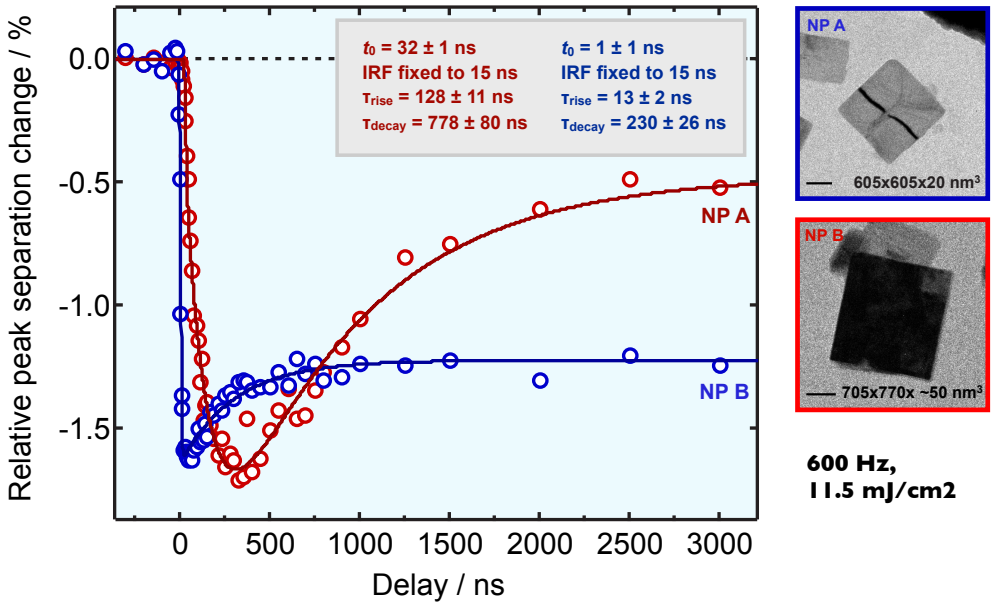

Figure S4

Fig. S5a compares the reciprocal and real-space dynamics for particle NP B. It shows identical rise and decay times. The real-space expansion (Fig. S5b) is approximately isotropic along both particle dimensions. Both observations indicate that the particle can freely expand without friction at the interface (e.g. due to stacking of particles).

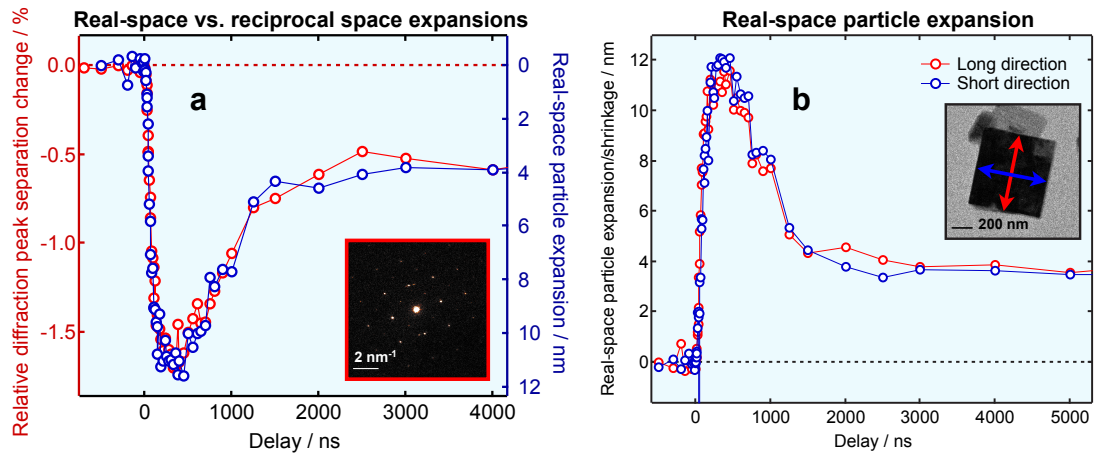

Figure S5

S5 Non-equilibrium phase-transition simulations

Phase-transition simulations allowed us to estimate the magnitudes and time scales of the observed spin crossover dynamics and to propose the non-equilibrium phase transition model proposed in the main text (Fig. 2c). A short description of the simulations follows below; a more detailed description will be published in a forthcoming article.

The aim of the heat diffusion calculations is to estimate the laser-induced temperature jumps in the graphite substrate and the nanoparticle and the ensuing time-resolved spin crossover efficiencies. We assume that the direct photo-excitation channel that leads to HS population can be neglected due to the low optical cross sections. We thus consider the situation of three objects in thermal contact: the nanoparticle (500x500 nm^2, 50 nm thickness), the graphite thin film (7.5x7.5 um^2, 3 nm thickness) and the Cu frame, which is assumed to act as a heat sink at constant temperature (90 K). Upon excitation, heat is promptly generated in both graphite and the nanoparticle according to the absorption cross-sections, sample thickness, and heat capacities at 90 K. We assume thermalization in both graphite and the particle is very fast (faster than the excitation pulse).

The optical cross section of the nanoparticle is not exactly known. Typical extinctions for MLCT transitions in transition-metal complexes are 10000 $M^{-1}cm^{-1}$, but because the laser polarization makes and angle of only several degrees with the transition dipole moment (aligned along the Fe-pyrazine axis), the absorption in the present case is expected to be much lower. For an extinction of 1000 $M^{-1}cm^{-1}$, a fluence of 10 mJ/cm^2, a heat capacity of 300 $JK^{-1}mol^{-1}$ and a particle thickness of 50 nm, the intra-particle temperature jump is 30 K. This is not enough to induce the spin crossover thermally, but it does add to the total temperature increase and needs to be taken into account. The laser energy was deposited as a Gaussian profile in space and time (FWHM 30 um, 7 ns).

The following equation

$$\frac{dQ}{dt} = C_p \cdot \frac{dT}{dt} = k\nabla^2 T - k'\Delta T - \Delta H \frac{df_{HS}(T,t)}{dt}$$

was solved numerically for an *x,y* grid with mesh size 500 nm. The asymmetry of the nanoparticle position with respect to the Cu frame was taken into account. It was verified that the calculation for mesh size of 500 nm gave the same result as one with smaller mesh sizes (e.g. 200 nm).

The enthalpy change of the spin crossover reaction was explicitly taken into account in the heat transfer calculation. Here it is assumed that the enthalpy change is directly proportional to the change in HS/LS fractions, with a total enthalpy change of ΔH = 21 kJ/mol for 100% conversion. The entropy change is adjusted to ΔS = 85 J/K/mol to match the temperature dependent diffraction measurement, under the assumption that the diffraction signal change is directly proportional to the fraction change (excluding thermal expansion). The total temperature-dependent heat capacity C_p of the nanoparticle becomes

$$C_p = \frac{dH}{dT} = (1-x)C_{p,l} + xC_{p,h} + \frac{dx}{dT}\Delta H$$

with C*p,l* and C*p,h* the heat capacities of the pure low-and high-spin states (assumed to be the same and fixed to 250 J/mol/K as derived from the DSC measurements), and x is the high-spin fraction. Due to the phase transition, the heat capacity increases around the phase transition temperature, i.e. instead of change the temperature, the thermal energy is used for the spin crossover.

The time-resolved HS fraction is obtained by incorporating the rate constants for LS →HS (k_l) and HS →LS (k_h) conversion, according to

$$\frac{dx}{dt} = k_l(1-x) - k_h x$$

k_h was measured optically as a function of temperature below the phase transition and an Arrhenius analysis provides the full temperature dependence according to

$$k_h = A \cdot e^{-E_a/RT}$$

and k_l and k_h are related by

$$k_l = K \cdot k_h$$

with

$$K = e^{-\Delta G/RT} = e^{\frac{\Delta S}{R} - \frac{\Delta H}{RT}}.$$

S6 Beam profiler camera

To follow the power and pointing stability of the pump laser beam in-situ, a beam profiler camera was installed along with the second-generation ultrafast electron microscope at Caltech. Briefly, a part of the excitation beam to the specimen in the microscope is picked up using a beam splitter after the focusing lens. The beam profiler camera is positioned at the image plane of equivalent distance to the specimen inside the microscope. If necessary, the power and position of the pump beam were adjusted to keep a consistent pump beam condition on the specimen according to that captured on the camera.

References

[1] I. Boldog, A. B. Gaspar, V. Martinez, P. Pardo-Ibañez, V. Ksenofontov, A. Bhattacharjee, P. Gütlich, J. A. Real, *Angew. Chem. Int. Ed.*, **2008**, *47*, 6433.